

**Thermal hysteresis and seeding of twisted fibers formed
by achiral discotic particles**

DASTAN, Alireza <<http://orcid.org/0000-0002-0967-4672>>, FRITH, William J.
and CLEAVER, Doug <<http://orcid.org/0000-0002-4278-0098>>

Available from Sheffield Hallam University Research Archive (SHURA) at:

<https://shura.shu.ac.uk/17084/>

This document is the Accepted Version [AM]

Citation:

DASTAN, Alireza, FRITH, William J. and CLEAVER, Doug (2017). Thermal hysteresis and seeding of twisted fibers formed by achiral discotic particles. *The Journal of Physical Chemistry B*, 121 (42), 9920-9928. [Article]

Copyright and re-use policy

See <http://shura.shu.ac.uk/information.html>

Thermal Hysteresis and Seeding of Twisted Fibers Formed by Achiral Discotic Particles

Alireza Dastan,[†] William J. Frith,[‡] and Douglas J. Cleaver^{*,†}

**Materials and Engineering Research Institute, Sheffield Hallam University, Howard Street, Sheffield S1 1WB, UK*

†Unilever Discover, Colworth Laboratories, Bedfordshire MK44 1LQ, UK

E-mail: d.j.cleaver@shu.ac.uk

Phone: +44-114-225-3055

Abstract

In this paper, Molecular Dynamics simulations of simple disc-shaped particles are used to investigate the free self-assembly of defect-free fibers. Depending on the choice of particle shape and interaction strength, the formed fibers are reproducibly either straight or, for reasons of packing efficiency, spontaneously chiral. As they grow radially, increasing stresses cause chiral fibers to untwist either continuously or via morphological rearrangement. It is also found that, due to the kinetics of fiber initiation, the isotropic solution has to be significantly supercooled before aggregation takes place. As a result, the thermal hysteresis of one formed fiber extends to 13.9% of the formation temperature. In the presence of a three-thread seed cluster of 15 particles, however, monotonic fiber growth is observed 9.3% above the normal formation temperature. Thus, as in many experimental systems, it is the kinetic pathway, rather than the thermodynamic stability of the final assembly, that dominates the observed behavior.

Introduction

There are many areas in which fibers play a key role. In some scenarios, fiber formation is highly favorable such as when it promotes secondary processes in various biological and non-biological applications. Behaviors in this category include examples from tissue engineering,^{1,2} stem cell differentiation³ and gel development.^{4–6} On the other hand, fiber formation is also a key feature of many diseases. Here, fiber growth is considered unfavorable and there is interest in being able to arrest or control it. Central to this category are “amyloid fibers”, insoluble neurotoxic fibrils formed from soluble proteins but resistant to degradation.⁷ Although there are some reports of functional amyloids which contribute positively to human health or technological applications,^{8–11} deposit of amyloid fibers is more commonly associated with various syndromes, such as Alzheimer’s disease, for each of which a particular protein or peptide makes up the basic self-assembling unit or building-block. Whilst there is evidence that, in infectious Prion diseases such as kuru and bovine spongiform encephalopa-

thy, consumption of amyloid fibers is linked to the onset of symptoms,¹² the mechanisms linking ingestion to aggregation and growth of fibrous plaques are not well understood.

Another, more general, perspective on this topic is raised by continua which are themselves comprised of sub-elements such as deformable fibers, filaments or sheets. Here, the inherent properties (mechanical, electrical, optical, ...) of the sub-elements combine with details of packing, bonding and topology to achieve key functionalities. Such capabilities are exploited in a plethora of organic and synthetic systems such as shells, organelles, proteins, nanotube assemblies and complex laminates.¹³ As such materials form, interplay between their competing growth modes, radial constraints and size- or response-dependent morphological changes of their various twisted components is intrinsic to system success.^{14,15} Further complication arises in the aggregation of such objects, however, since, in general, this involves a hierarchy of sub-aggregates and, so, cannot be described purely in terms of single-molecule mechanisms. As with the kinetic cascades realised to achieve accelerated growth in various bio-mineralisation processes,¹⁶ it is inherent in hierarchical self-assembly that the presence of a free energy barrier between each stage introduces possible complexities such as trapping in metastable states or competition between alternative kinetic pathways.¹⁷

These complications are exemplified by the study of Gosal et al. which found that, depending on pH and concentration, β_2 -Microglobulin may form either worm-like fibrils or long, mature amyloids.¹⁸ Each of these final morphologies was found to involve a distinct kinetic pathway. In one, rod-like fibrils and, eventually, worm-like assemblies were formed by a reversible, non-nucleated mechanism, the end product (the worm-like fibrils) being shown to be a kinetically trapped assembly. In the second, long amyloid fibers were formed by nucleation-driven growth involving a kinetic lag-phase. However, addition of small pre-formed fibers to this system promoted the formation of the long amyloid fibers in conditions that would normally correspond to the first pathway. Thus, seeding was demonstrated to be a viable mechanism for switching between dominant growth pathways, through manipulation of kinetic barriers. In a related experimental study on disc-shape aromatic aramid

molecules, Huang et al.¹⁹ observed that hexagonally packed threads form nanofibers. Here, it was suggested that hexagonal, planar clusters of seven discotic molecules formed in the early stages, and that these subsequently stacked to form fibers. Engelkamp et al.,²⁰ however, suggested a different pathway for the self assembly of discotic molecules with chiral tails into left-handed, twisted bundles and, ultimately, gels. Here, each bundle was found to comprise two right-handed twisted fibers which were themselves stabilised through the mutual attractions between their aromatic disc cores. Gels then developed via a hierarchy of super-coiled threads, with the helicity changing handedness at each generation.

Several previous modelling and simulation studies have been performed to investigate the self-assembly of fibrous structures from a theoretical perspective.^{21–24} Interpretations based on classical nucleation theory have proved applicable to coarse-grained simulations involving single-particle aggregation of amyloid fibers. For example, in the work of Zhang and Muthukumar,²² two types of lag time were observed: one, seen in systems with moderate concentration and low temperature, did not respond to the presence of seeds, whereas the other, found at low concentration and high temperature, could be eliminated by seeding. However, Auer and co-workers then showed that, to take into account considerations such as the absence of differential scaling between surface and bulk free energy terms as a function of fiber length, it is necessary to generalise the nucleation theory approach for these systems.^{23,25} Other approaches to modelling the development of highly elongated stacks of molecules have described the observed behavior in terms of a hierarchy of interacting processes and structures.^{21,26–29} Such hierarchies can, though, introduce kinetic complications relating to either the high free energy (and associated time lag) of key intermediate structures or the high stability of disruptive intermediates, leading to reduced yield or even kinetic arrest.³⁰ Kinetic trapping has been reported experimentally in the supramolecular polymerization of perylene bisimide, a molecule with a planar core,³¹ which shows a time-lag in formation and thermal hysteresis between cooling and heating. Shape anisotropy of the underlying molecular or colloidal building blocks can also add to the complexity of for-

mation and growth mechanisms. Orientational order metastability is one example of this complexity, discotic colloidal particles forming small ordered strands at the early stages of self-assembly from isotropic solution, regardless of the growth pathway or final structure.³² A recent analysis of assembly processes in chromonic liquid crystal systems³³ usefully differentiates between isodesmic stacking and threshold-associated, large-scale aggregation in interpreting the behaviours exhibited by experimental systems.

The aims of this study are to determine whether fiber formation behaviors are accessible, in a reproducible way, to molecular simulation and, if so, to gain clearer insight into the competing kinetic and thermodynamic effects that are apparent from related experimental systems. To this end, the self-assembly is considered of twisted and straight fibers from achiral, discotic (oblate ellipsoidal) building-blocks using conventional Molecular Dynamics (MD) simulation. In this, computer simulation methods such as meta-dynamics and forward-flux-sampling, which have been developed to investigate rare events (such as nucleation) and explore reaction pathways, are consciously avoided. This is because they also prescribe the form of any final aggregate and (importantly) bias any intermediate structures and, thus, the associated hierarchical self-assembly pathways. The study is restricted, therefore, to the more prosaic, but bias-free, procedures adopted in previous simulation studies^{28,34} of fiber-formation from an isotopic precursor phase.

Having established a systematic route to observing free self-assembly of fibers, the study goes on to investigate both the resulting aggregates and the extent to which thermal hysteresis and seeding can also be captured in this simple model system. From this, the fiber pitch, which is a fully emergent, supra-molecular length-scale, proves to be a viable indicator of aggregate character. Also, very large thermal hysteresis is found, due, in the main, to the absence of an accessible kinetic pathway from the supercooled isotropic state. Introduction of a small but permanent seed cluster proves sufficient to open this limiting bottleneck, the extent of the shift in fiber-forming temperature varying in proportion to seed size. Thus, despite its inherent restrictions of length- and time-scale, MD simulation proves capable of

capturing a remarkably broad range of behaviors pertinent to this directed self-assembly process.

Simulation Procedures

In this paper, the initiation and growth of free self-assembling fibers are investigated through MD simulation of generic disc-shaped ellipsoidal particles. The interactions between particles are governed by the Gay-Berne (GB) potential, a well established coarse-grained model which generalises the 12-6 Lennard-Jones interaction to anisotropic particle shapes and incorporates dependence on the particle orientations by considering a unit vector, $\hat{\mathbf{u}}$, attached to the symmetry axis of each particle.^{35,36} The liquid crystalline phase behaviour of this model system were established by Bates and Luckhurst,³⁷ with later work identifying localised helical structures in the columnar mesophase.³⁸

The GB interaction potential for two discotic particles, U^{dd} , is given by:³⁷

$$U^{\text{dd}} = 4\epsilon(\hat{\mathbf{u}}_i, \hat{\mathbf{u}}_j, \mathbf{r}_{ij}) \left[\left(\frac{\sigma_f}{r - \sigma(\hat{\mathbf{u}}_i, \hat{\mathbf{u}}_j, \mathbf{r}_{ij}) + \sigma_f} \right)^{12} - \left(\frac{\sigma_f}{r - \sigma(\hat{\mathbf{u}}_i, \hat{\mathbf{u}}_j, \mathbf{r}_{ij}) + \sigma_f} \right)^6 \right]. \quad (1)$$

Here, $\epsilon(\hat{\mathbf{u}}_i, \hat{\mathbf{u}}_j, \mathbf{r}_{ij})$ and $\sigma(\hat{\mathbf{u}}_i, \hat{\mathbf{u}}_j, \mathbf{r}_{ij})$ are energy and shape functions, which are dependent on the relative orientations and positions, \mathbf{r}_{ij} , of the particles. The inter-particle separation and thickness of the discs are r and σ_f , respectively. The analytical expressions for ϵ and σ are available throughout the literature,^{35,37} and so are not reproduced here.

The main anisotropies of the GB potential are characterised by two parameters. The first of these is the shape parameter, κ , which is equal to the particle length-to-breadth ratio. The second is the energy parameter, κ' , which is given by the ratio of the potential well-depth at edge-edge configuration to that in face-face orientation (Figure 1). All systems considered here employ particles which are parameterised to be oblate, or disc-shaped, ellipsoids and to have energetic preference to stack face-to-face. This evokes the $\pi - \pi$ interaction of the aromatic cores of discotic liquid crystals and, more particularly, lyotropics which exhibit

chromonic self-assembly.³⁹ Two other constants, μ and ν , are used in the calculation of the ϵ function,³⁵ so that the full potential is commonly characterised in terms of 4 parameters and written as $\text{GB}(\kappa, \kappa', \mu, \nu)$. Here, a range of κ and κ' values have been explored, but μ and ν have been fixed at their usual values of 1 and 2, respectively.³⁷ As a result, the edge-edge well-depth is 3.3, 2.63 and 2.103 for κ values 0.3, 0.345 and 0.4, respectively. For each disc shape, the face-face interaction is then controlled by the κ' parameter. Figure 1 shows plots of the $\text{GB}(0.345, 0.15, 1, 2)$ potential for two relative particle orientations. Following convention,⁴⁰ the potential was cut and shifted at a spherical cut-off radius of 1.7 disc diameters, in order to reduce the computational costs.

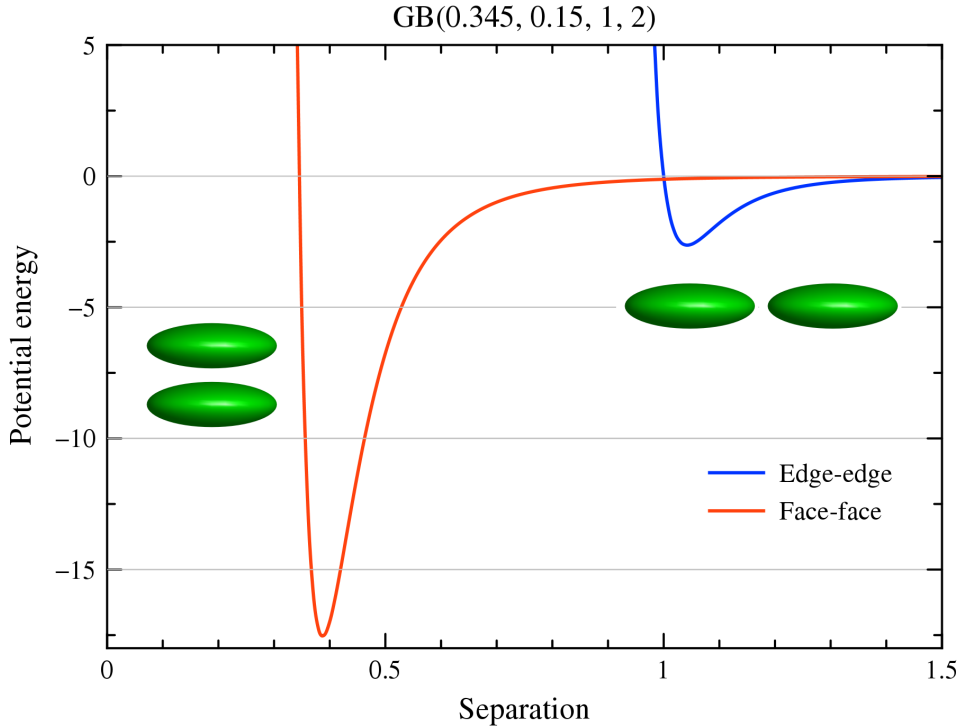


Figure 1: GB potential energy plots for face-face and edge-edge configurations of $\text{GB}(0.345, 0.15, 1, 2)$. The separation is presented in reduced unit which is the disc diameter.

The work presented here builds upon and expands that of Prybytak et al.,²⁸ wherein a two-component mixture of GB discs and spherical Lennard-Jones particles was simulated to study fiber self-assembly. Here, however, no spherical particles have been utilised and the simulations have only involved GB particles. This gives both greater clarity of interpretation,

due to the reduced parameter space of the model, and increased run times, because of the associated computational savings.

In the first series of simulations presented here, 15 different systems have been considered, characterised by three values of κ (0.3, 0.345, 0.4) and five values of κ' (0.05, 0.1, 0.15, 0.2, 0.3). For each of these parameter combinations, a 3d periodic, cubic system of 600 discs has been cooled at a reduced number density of 0.075, that is with a box length of 20 disc diameters. Here and subsequently, conventional reduced units are used in presenting simulation data,^{28,40} the disc diameter being the basic unit of length.

In all cases, initial equilibration runs performed at high temperatures resulted in isotropic and homogeneous configurations, with no translational or orientational order. Temperature decrements of 0.1 were used at high temperature, but these were reduced to 0.01 as each fiber-formation temperature was approached. At each temperature, 3×10^6 MD time-steps of 10^{-3} time units were performed in the constant NVT ensemble, a Nosé-Hoover thermostat⁴¹ being applied for both translational and rotational motions, independently, to maintain the desired temperature. The equations of particle motion were solved using the NOSQUISH integration algorithm.^{42,43} For the temperatures at which fiber formation was observed, runs were extended to tens of millions of time-steps so that a steady state was achieved. Also, as described below, a small number of highly extended runs were performed at other temperatures.

As well as standard thermodynamic data and the orientational order parameter,⁴⁴ systems were assessed in terms of the state of self-assembly exhibited. The latter was achieved through two levels of cluster identification.⁴⁰ Stacks, or "threads", of discs were identified based on groupings of particles with mutual separation of 1.5κ or less. From this, it was possible to trace the population of monomers, stacks of two particles (dimers), stacks of three (trimers) etc. Multi-thread objects, involving lateral association of two or more threads, were then characterised by distances of up to 1.1 between particles in different threads. From this, it was possible to trace the populations of single threads, pairs of associating

threads (twins), assemblies of three threads (triplets) etc. Through this characterisation, it was straightforward to assess the establishment of a steady-state, in systems above the fiber forming temperature, by the time-stability of the observed stack-length and thread-number distribution functions. Further, as and when fiber self-assembly did occur, this was readily apparent from slow but monotonic drifts in, for example, the number of free monomers.

In the second set of simulations presented here, the $\kappa = 0.345$, $\kappa' = 0.15$ system was studied in more detail so as to investigate a) its thermal hysteresis and b) the sensitivity of its fiber formation to seeding. To study the hysteresis, the final fiber formed on cooling this system was warmed in increments of 0.01 until it fully dissolved. As previously, equilibration was gauged at each temperature by the stabilisation of the fiber size and the number of free monomer particles in the supporting fluid. Typical run-lengths here were 3×10^6 MD time-steps. To study seeding, further full cooling sequences were undertaken of systems loaded with a single permanent cluster consisting of, respectively, 1, 2 or 3 threads of 5 particles. The relative positions and orientations of the particles in these permanent seed clusters were taken from the core of the fiber formed in the original simulation with these parameters. In these seeded cooling runs, the integrity of the seed clusters was maintained by increasing the mutual well-depths of seed particles by a factor of 10, whereas normal interactions were applied between seed particles and the remainder of the system. Here, the time step was reduced to 5×10^{-4} , and run-lengths were extended to at least 5×10^6 steps.

Results and Discussion

Fiber Self-assembly

On cooling initially isotropic systems of 600 GB discs from high temperature, systematic changes were observed in the steady state proportions of particles identified either as monomers or as being in stacks of various lengths. This behavior is exemplified by the data shown in Figure 2 for the system $\kappa = 0.345$, $\kappa' = 0.15$, which indicates how the monomer

number dropped and the numbers of particles in dimer and trimer stacks increased as temperature was decreased from 1.75 to 1.52. At each of these temperatures, a dynamic equilibrium was achieved in the monomer, dimer and trimer numbers. Within each simulation, this was characterised by continuous making and breaking of highly mobile threads (dimers, trimers, tetramers, etc.) and, occasionally, short-lived, multi-thread objects.

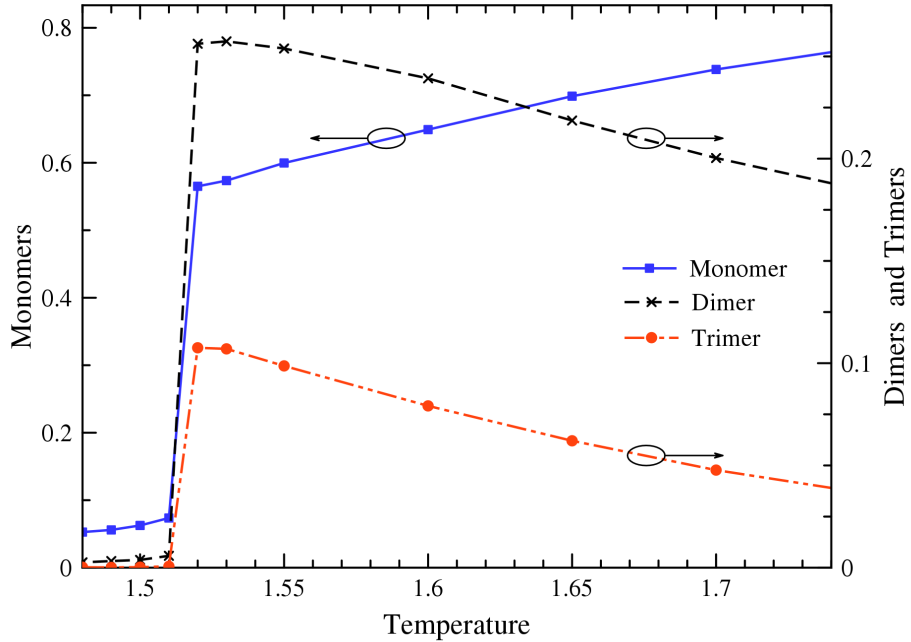


Figure 2: Normalized numbers of discs in the form of monomers, dimers and trimers, averaged over the production phases (last 10^6 steps) of a cooling sequence of the $\kappa = 0.345$, $\kappa' = 0.15$ system without seed. Arrows indicate the associated vertical axis for each data set. Maximum Standard Deviation of data is 2.7%, and is not shown for simplicity.

At $T=1.51$, rather than stabilising to fixed values, as at all higher temperature runs, the populations of particles identifiable as monomers or as being in short threads showed slow but concerted decay, after an initial lag time (1-2 million MD steps). This decay was indicative of the initiation and growth of a single large assembly (see Figure 8 for the size of the cluster in a cooling down process), over a timescale of several 10^6 MD time-steps. The resultant assembly, a multi-thread, twisted fiber, is depicted in Figure 3 . As indicated in Figure 2, the cumulative number of monomers, dimers, trimers etc. dropped below 10% at

this temperature, meaning that the final fiber which developed at $T=1.51$ comprised over 90% of the discs involved in the simulation. Like the fiber described in our previous paper,²⁸ this object comprised a straight central thread, three complete layers of 6 threads each and a partial fourth layer. As previously observed, the spontaneous twist in this fiber resulted as a compromise due to the frustration which results when threads attempt to both pack hexagonally and interdigitate with their neighbors.⁴⁵ Since there are no chiral terms in the inter-particle interactions used in this study, both left-handed and right-handed fibers have been observed with equal likelihood in these simulations. In the early stages of each fiber growth simulation, repeated changes of handedness were observed, but these reduced with increase in number of threads and fully arrested once the fiber had seven threads. Thus, a different final fiber handedness from that shown in Figure 3 was readily achievable by repeating this fiber-forming simulation with different initial configurations.

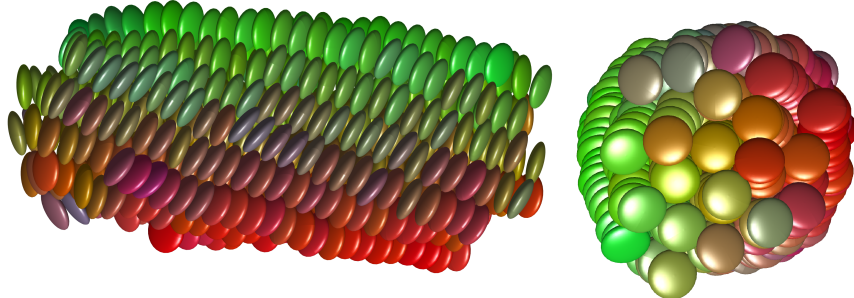


Figure 3: Two views of the self-assembled fiber formed at $T=1.51$ ($\kappa = 0.345$, $\kappa' = 0.15$). The discs are color-coded based on their orientations. The slight change of color within individual threads is an indication of twist and writhe in the structure. Both hexagonal local packing of threads and defect-free interdigititation of particles in neighboring threads are apparent.

To further investigate the propensity for fiber formation in these systems, extended runs were performed at $T=1.52$, 1.53 and 1.54. At $T=1.52$, a dynamic equilibrium persisted for 6×10^6 MD time-steps, after which fiber formation was eventually signalled by a comparatively fast reduction (over $\simeq 10^6$ MD time-steps) in free monomers. At $T=1.53$, the isotropic state persisted for nearly 50×10^6 MD time-steps after which fiber formation was again seen.

However, at $T=1.54$, the system remained isotropic throughout a long run of 300×10^6 MD time-steps.

Repeating the gentle cooling procedure for the other 14 combinations of shape anisotropy parameter κ and energy anisotropy parameter κ' resulted in the observation of rapid-fiber-onset temperatures in all cases. These are plotted in Figure 4. When each fiber formation was triggered, it went on to consume a significant number of particles in the simulation. Thus, the formed fibers shown in Figure 5 were the only aggregates in each simulation when the observables reached their steady-state values. In all cases, these final fibers comprised between 75 and 97% of the particles in the simulation. Given that κ' is inversely proportional to the strong face-face interaction strength (the dominant interaction here), it is reasonable that, for fixed κ , these temperatures should follow hyperbolae. The aspect ratios of the formed fibers show a clear trend, being long and thin for low κ' but progressively shorter and fatter on increase of this parameter, similar to the behavior observed in previous fibril-forming simulations with a more coarse-grained model.²² This can be explained qualitatively by the competing lateral and longitudinal growth rates in these systems, with longer fibers being associated with stronger face-face interactions between the constituent discs. The final formed fibers varied between 15.7 disc diameters (for $\kappa = 0.4$, $\kappa' = 0.05$) and 6.5 disc diameters (for $\kappa = 0.3$, $\kappa' = 0.3$) in length. Thus, in all cases, the fibers were significantly shorter than the simulation box size and, so, were not influenced by the periodic boundary conditions. Whilst the smooth variation in fiber-onset temperatures seen in this graph suggests consistent behavior for all 15 systems, snapshots of the final fibers (Figure 5) indicate that this masks some important changes. For example, for high κ and low κ' , that is more spherical particles with strong face-face interactions, the fibers formed were straight, rather than twisted.

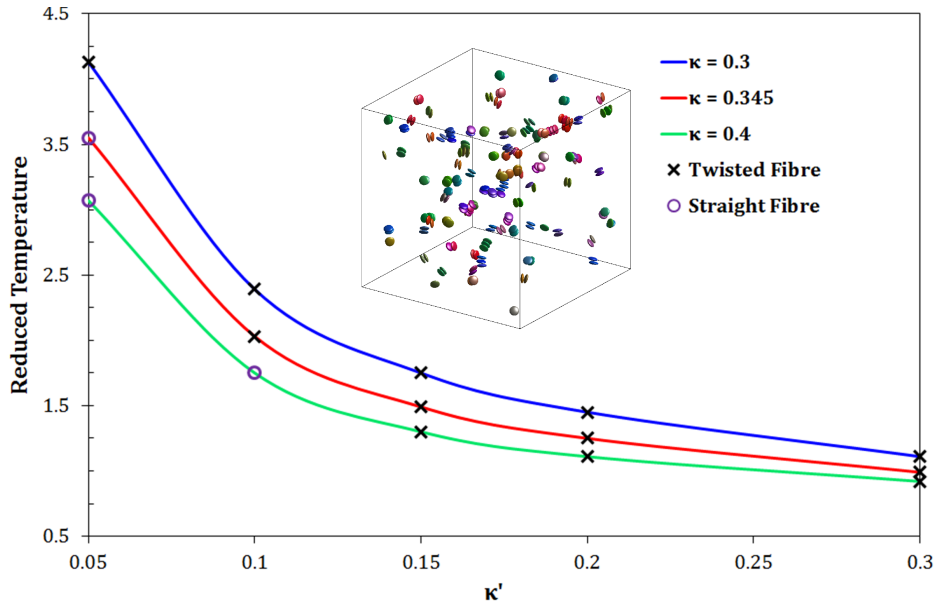


Figure 4: Fiber-onset temperatures on cooling from isotropic, for systems with a range of particle shape and energy anisotropies. For each κ value, the system above the associated curve is isotropic. A snapshot of the $\kappa = 0.345$, $\kappa' = 0.15$ system at $T=1.6$ (with monomer discs omitted, for clarity) is illustrated as an example of behavior in this region. No dominant structure is apparent, but numerous short threads and a few multi-thread clusters are seen.

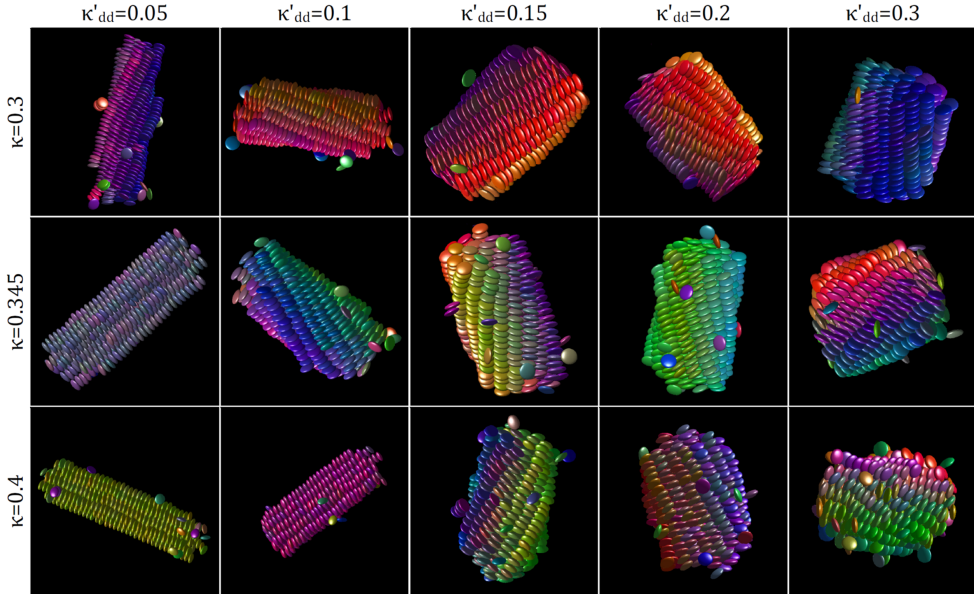


Figure 5: Snapshots of the final formed fibers, on cooling from isotropic, for systems with a range of particle shape and energy anisotropies, κ and κ' . For clarity, snapshots are zoomed in to fill each box, rather than all being to scale.

Fiber pitch lengths for each combination of κ and κ' , determined by fitting individual thread loci to helices using the procedure suggested by Eberly⁴⁶ and averaging over threads and configurations (over 10^6 time-steps, where possible) are plotted in Figure 6. In cluster pitch calculation, it was assumed that the axis of each helix was the director of the cluster⁴⁴ and passed through its center of mass. However, as is apparent from the reported fiber- and pitch-lengths, it was not possible to observe a complete pitch in the systems considered here. Figure 6 shows that, for $\kappa=0.3$, the pitch grew slightly from 35 disc diameters for low κ' to 40 for $\kappa'=0.3$. Generally, a similar trend was observed for the fiber radius. This indicates that fiber growth promoted gradual unwinding of the twisted structures, whose early stage pitch lengths were dictated by the optimal packing of seven interdigitating threads. Increasing disc thickness to $\kappa=0.345$ led to slightly lower pitch values because these particles had to adopt larger tilt angles to achieve the necessary interdigitation. However, for most $\kappa=0.345$ systems, the κ' -dependence was the same as that observed for $\kappa=0.3$. The one exception to this was the system with the strongest disc-disc affinity ($\kappa'=0.05$) which grew as a straight (i.e. infinite pitch) fiber. This, though, is entirely consistent with the zero-temperature calculations of Chakrabarti et al.,⁴⁵ which identified an equivalent crossover when determining the relative stabilities of isolated, multi-thread clusters of discs.

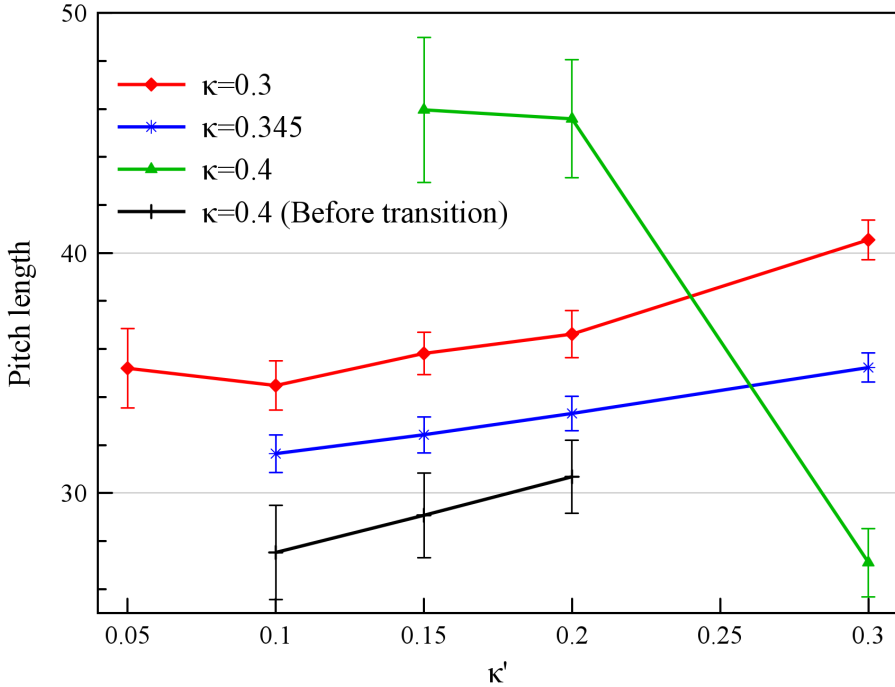


Figure 6: Pitch of the formed fibers as a function of energy anisotropy, κ' , for three particle shape anisotropies κ . For $\kappa=0.4$, pitch lengths adopted prior to unwinding are labelled as "Before transition". Straight threads (with infinite pitch) are not marked. The error bars show \pm Standard Deviation of cluster pitch averaged over the production phases.

Fiber pitch increased with κ' in these systems in order to accommodate the thread stresses associated with corresponding increases in fiber radius. In the defect-free fibers formed here, interdigitation imposes a constraint that all threads have identical axial (i.e. parallel to the fiber axis) strain. Additionally, since the loci of threads in each successive layer differ by a torsion angle, strains along local thread axes must grow with their writhe radii - Grason has argued that thread stresses in twisted fibers increase as r^4 .¹³ In order to maintain axial mechanical stability in these simulations, therefore, central threads necessarily underwent net compression, to balance the extension of the outer threads. Growing tangential strains, correspondingly, caused concerted increase in fiber pitch length.

As illustrated by the order parameter time-lines shown in Figure 7, even richer untwisting behaviour was found for the $\kappa=0.4$ systems. These data indicate the instantaneous orientational order (i.e. the nematic order parameter⁴⁴) of the particles within each growing

fiber. Thus, for $\kappa'=0.3$ the orientational order can be seen to have decayed as the strongly aligned early-stage cluster developed coherent twist and writhe in its constituent threads. For $\kappa'=0.05$, in contrast, the fiber grew as a straight object, and its order parameter remained over 0.95 throughout. Between these two limiting behaviors, however, size-dependent transitional behaviour was apparent - at $\kappa'=0.1$, initial order parameter decay was arrested, reversed, and ultimately exhibited a jump to a high constant value; and at $\kappa'=0.15$ and 0.2, the order parameter dropped to 0.6-0.7 before recovering to a steady state of 0.8. Pitch values calculated before and after these untwisting transitions are both plotted in Figure 6. These suggest that pre-transition, the pitches of the formed fibers were consistent with those adopted by thinner discs. As they grew further, however, their increasing fiber radii triggered either complete straightening (for $\kappa'=0.1$) or substantive untwisting to a pitch of 45 disc diameters (for $\kappa'=0.15$ and 0.2). The deviation of the $\kappa'=0.3$ system from the general trend of pitch length increase with κ' may be due to it being the smallest of the fibers observed.

Size-dependent morphological changes of growing twisted structures have been the focus of recent work exploring geometric frustration in chiral filament bundles,¹⁴ but we are not aware of any previous observations by MD simulation. We shall, therefore, return to this issue in a future publication focussing on system-size dependence and fiber-formation kinetics.

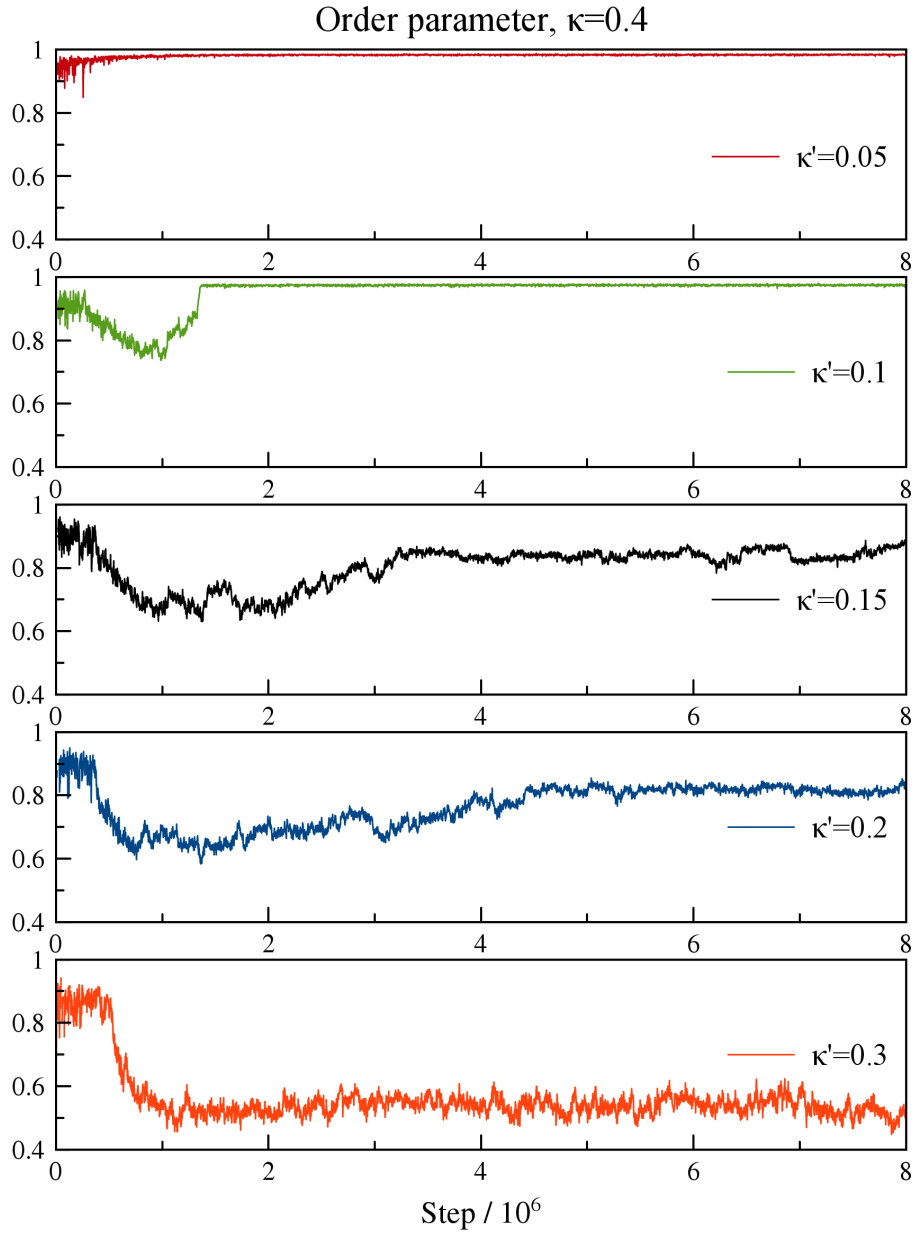


Figure 7: Time lines of the orientational order parameter of the particles in the growing fibers formed by $\kappa=0.4$ systems with a range of energy anisotropies, κ' . All graphs are drawn from the beginning of the fiber growth phase and any latency prior to fiber initiation (a few million MD time-steps) is omitted.

Thermal Hysteresis and Seeding

On heating the $\kappa = 0.345$, $\kappa' = 0.15$ system fiber, particles were shed into solution at every temperature increment, but a steady state was readily achieved at each step. This is

depicted on the "Heating up" branch of the overall cluster size graph, Figure 8. Although it progressively reduced in size on heating, as illustrated in the figure, the fiber retained its integrity up to $T=1.72$, that is 13.9% above the temperature at which rapid formation was observed ($T=1.51$). This very large thermal hysteresis is far greater than which would be expected for the biphasic gap in typical soft matter systems - it corresponds to about 40°C for a room temperature process. This, coupled with the fact that, when fiber formation did occur on cooling from the isotropic state it involved aggregation of over 90% of the simulated particles, is strongly suggestive of bistability.⁴⁷ In particular, it signals that the cooling branch incurred kinetic trapping in the metastable isotropic state. It is also reminiscent of experimental observations such as the large-scale assembly of the chromonic liquid crystal IR-806,⁴⁸ and the polymerization of perylene bisimide into a long 1D aggregate,³¹ where the thermal hysteresis was shown to be in the range of 3.1% and 8.6% above the formation temperature, depending upon concentration and the nature of the solution.

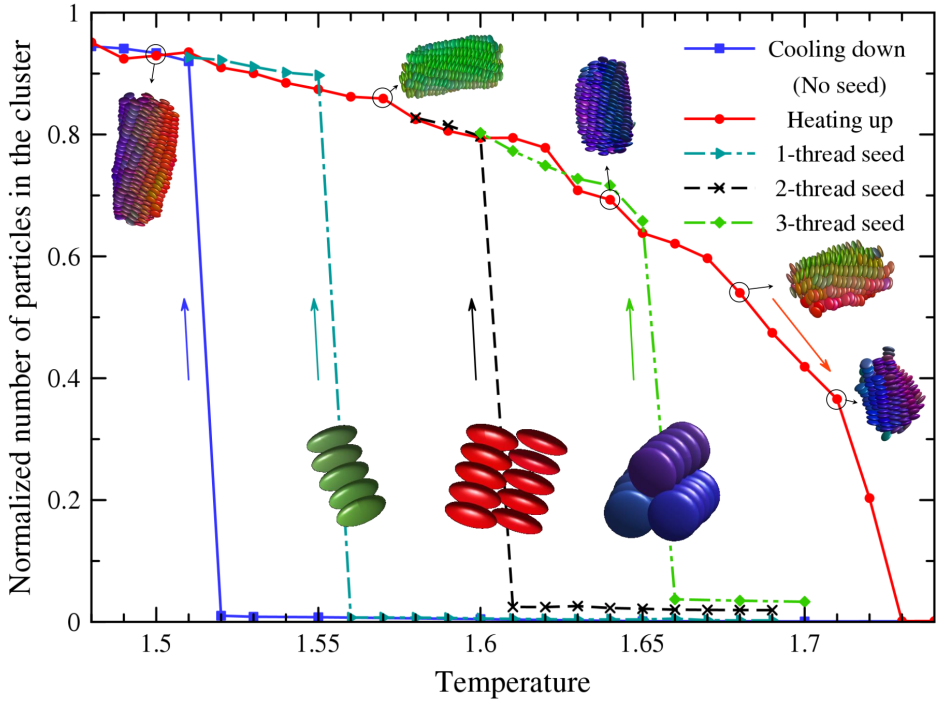


Figure 8: Averaged proportion of particles in the biggest cluster on incrementally cooling and heating various $\kappa = 0.345$, $\kappa' = 0.15$ systems of 600 GB discs. The configuration of discs used to seed certain of the cooling sequences is shown on the corresponding curve. The diminution of the fiber on heating is illustrated by snapshots obtained at different temperatures. Maximum Standard Deviation of data is 3% and occurs at $T=1.72$ on the heating curve.

Structural analysis data for a fiber on heating above its formation temperature ($T=1.51$) is presented in Figure 9. This shows that the pitch length remained virtually constant up to temperature 1.65 and then slightly dropped to about 90% of its original value before complete dissociation. Also, while particles dispersed from fiber and the cluster size became smaller, the number of threads remained nearly constant - indicating that the fibre shrinkage occurred from its ends, not laterally. This is confirmed by data for both the principal Moments of Inertia and the aspect ratio of the fibre. Snapshots of this heated fiber, given on Figure 8, also show that its length decreased while its diameter remained relatively unchanged. Thus, a sharp drop in the number of threads and, subsequently, the dissolution of the fiber was only seen when the temperature exceeded $T=1.71$, at which point the number of threads went below 19, i.e., the value representing three complete layers. Furthermore, this analysis

shows that, for $T \leq 1.71$, disaggregation was dominated by a single-particle process (i.e. monomers being shed from thread ends).

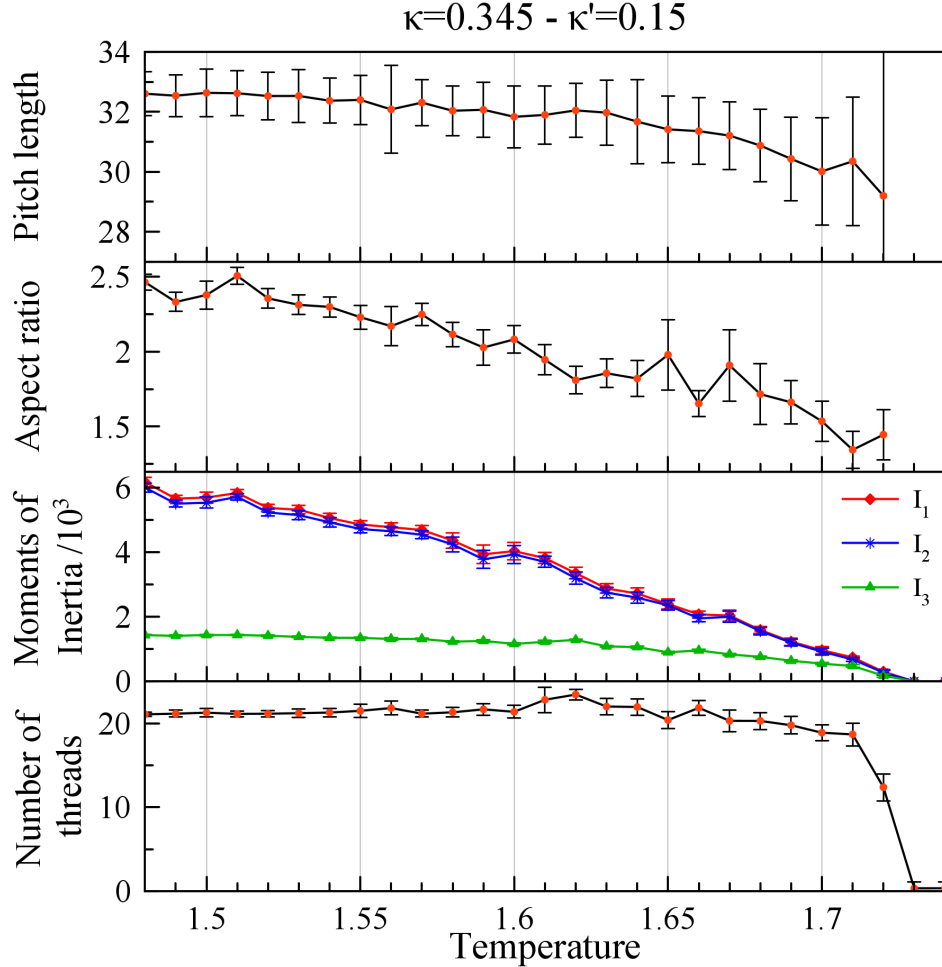


Figure 9: Averaged structural properties of the biggest cluster over the production phase in heating simulations of $\kappa = 0.345$, $\kappa' = 0.15$ system. The error bars show \pm Standard Deviation of sampled data.

Figure 8 also shows the temperature dependence of the steady-state aggregate size when the $\kappa = 0.345$, $\kappa' = 0.15$ system was cooled in the presence of a permanent seed clusters comprising, respectively, one, two or three 5-disc threads. This shows that the presence of each of these seeds had a significant effect on the fiber-formation. In each case, the fiber branch of the thermal hysteresis loop was accessed at a successively higher temperature - the fiber forming temperature being increased by 2.6%, 6% and 9.3% for the one-, two- and three

thread seeds, respectively. Equivalent behavior was found in further simulations involving a range of other seeds (not shown), the shift of the fiber-forming temperature generally being proportional to the number of discs in the seed. For seeds which had imprinted twist, the sense of chirality of the final fiber always matched that of the seed used.

In each of these examples of seed-enabled fiber formation, it is noteworthy that the resultant assembly achieved essentially the same cluster size as that of the heated fiber at the corresponding temperature. This suggests the existence of a well-defined "fiber state". Time-lines of the respective fiber formation processes (Figure 10) indicate that, while the presence of seeds made fiber formation viable at increased temperatures, the timescales associated with the assembly were extended, significantly in the case of the three-thread seed. That is, formation at higher temperatures led to both smaller cluster sizes (Figure 8) and slower self-assembly processes. This is consistent with the previous findings of Zhang and Muthukumar.²²

It is also apparent, from Figure 10, that fiber growth was essentially monotonic for all three of the seeded systems shown here and did *not* suggest coexistence between states with similar free energies. This provides yet more evidence that the fiber branch represents the thermodynamically stable state for much of the thermal hysteresis loop depicted in Figure 8, and that kinetic trapping, that is the absence of an accessible kinetic pathway, was central to these systems remaining isotropic down to the temperatures shown in Figure 4.

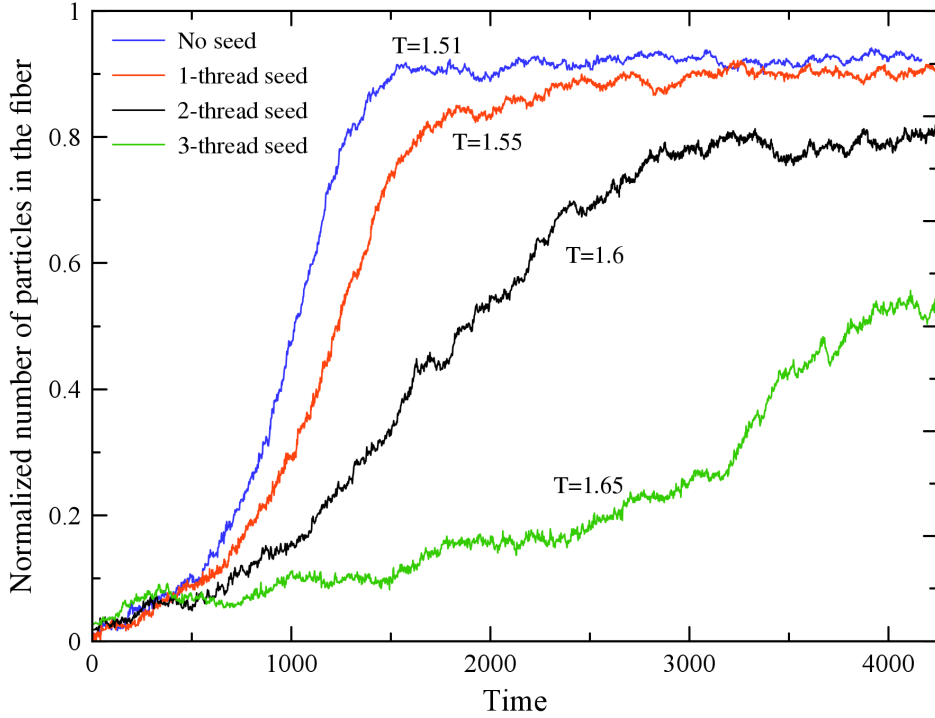


Figure 10: Normalized number of particles in the formed fiber in each investigated system versus reduced time ($\kappa = 0.345$, $\kappa' = 0.15$). To aid comparison, all graphs are drawn from the beginning of the fiber growth phase and any latency prior to fiber initiation (few millions MD time-steps) is omitted. The formation temperature for each system is written next to the associated graphs. The system with the 3-thread seed continued to grow beyond the time window shown here.

Conclusions

In this paper, MD simulation of coarse-grained discotic particles has been used to study the free self-assembly of defect-free, twisted and straight fibers. This approach has proven capable of capturing physical phenomena such as emergent chirality, which has eluded more coarse-grained models,²² whilst also accessing large time- and length-scale behaviours, such as geometrical frustration, that are not yet achievable by atomistic simulation. The results show that the fiber formation is fully reproducible and applies over a significant range of particle shapes and interaction strengths. The chiral fibers observed here have a pitch of 30-45 disc diameters, this pitch being a fully emergent, supra-molecular length-scale. For

some systems, untwisting of growing fibers has been observed, an apparent manifestation of the size-dependent morphological changes expected more generally in assemblies comprising chiral filaments.¹⁴ The pitch lengths observed in Figure 6 arise due to a combination of factors: 1) the tilt of particles in interdigitating, helical threads; 2) slight untwisting due to radius-dependent stresses; and 3) significant untwisting of fibers with low κ' , i.e. high thread bending rigidity. Further, the observation here of spontaneous "structural chirality", achieved through self-assembly of achiral objects, feeds into the ongoing debate on complex continua in which it is argued that the character and properties of any dense-phase material comprising such structures are highly sensitive to the interplay of intrinsic stresses and the packing efficiency of different hierarchical components.¹³ Whilst multi-fiber assemblies are beyond the scope of the current paper, our findings do indicate that they are likely to become accessible to molecular simulation approaches in the near future.

The fiber-formation process observed here is subject to kinetic trapping, the isotropic phase remaining indefinitely long-lived well below its window of thermodynamic stability. In this respect, these simulations are redolent of the chromonic liquid crystal IR-806, which forms a large aggregate on increase in concentration but shows no biphasic coexistence.⁴⁸ As such, the mechanism involved resembles those discussed by Collings and coworkers³³ in which small precursor assemblies are developed prior to full aggregation. From the range of simulations performed here, it is apparent that the fiber formation curves depicted in Figure 4 correspond to the temperatures at which the monomer number fails to achieve steady state until fiber growth is complete. As such, they represent the limit at which the cooled isotropic phase becomes absolutely unstable with respect to aggregate formation. Armed with this understanding, fiber formation has also been observed at higher temperatures, either through extending simulation times or introducing seed clusters. Whilst extending run times only achieved a modest rise in viable fiber-formation temperatures, seeding with permanent clusters yielded irreversible fiber-growth at significantly higher temperatures. Thus, identification and, through gradually increased seed sizes, systematic manipulation

of this key kinetic bottleneck proved a very effective means of controlling system behavior. Whilst Gosal et al. have successfully used seeding to steer the aggregation product of β_2 -Microglobulin systems,¹⁸ there would appear to be scope to use this approach more generally - provided that appropriate seed-clusters can be identified and controllably introduced to other kinetically-arrested aggregating systems.

Taken as a whole, these results indicate that the large thermal hysteresis apparent from Figure 4 is overwhelmingly due to kinetic, rather than thermodynamic, factors. The insensitivity of the fiber forming temperatures to the final structure - twisted or straight - is a further indication that the kinetic pathway, rather than the thermodynamic stability of the assembly formed, is the dominant consideration for these systems. This signals that, in the hierarchy of processes involved in full fiber self-assembly, it is the earlier stages (corresponding to objects such as the 5-15-disc seeds used in Section) that determine the stability limit of the super-cooled isotropic state. The specific details of this relate to the hierarchical cascade of self-assembly processes involved in this system's fiber growth - this will be described in detail in a future publication which will also consider morphological change and the effect of simulation system size.

Acknowledgement

A.D. gratefully acknowledges financial support from Unilever Discover.

References

- (1) Smith, L. A.; Ma, P. X. Nano-fibrous Scaffolds for Tissue Engineering. *Colloid Surf. B-Biointerfaces* **2004**, *39*, 125–131.
- (2) Guo, J.; Su, H.; Zeng, Y.; Liang, Y.-X.; Wong, W. M.; Ellis-Behnke, R. G.; So, K.-

- F.; Wu, W. Reknitting the Injured Spinal Cord by Self-assembling Peptide Nanofiber Scaffold. *Nanomed.-Nanotechnol. Biol. Med.* **2007**, *3*, 311–321.
- (3) Hosseinkhani, H.; Hosseinkhani, M.; Tian, F.; Kobayashi, H.; Tabata, Y. Osteogenic Differentiation of Mesenchymal Stem Cells in Self-assembled Peptide-amphiphile Nanofibers. *Biomaterials* **2006**, *27*, 4079–4086.
- (4) Sangeetha, N. M.; Maitra, U. Supramolecular Gels: Functions and Uses. *Chem. Soc. Rev.* **2005**, *34*, 821–836.
- (5) Zhou, M.; Smith, A. M.; Das, A. K.; Hodson, N. W.; Collins, R. F.; Ulijn, R. V.; Gough, J. E. Self-assembled Peptide-based Hydrogels as Scaffolds for Anchorage-dependent Cells. *Biomaterials* **2009**, *30*, 2523–2530.
- (6) Frith, W. J. Self-assembly of Small Peptide Amphiphiles, the Structures Formed and their Applications. (A Foods and Home and Personal Care Perspective). *Philos. Trans. R. Soc. A-Math. Phys. Eng. Sci.* **2016**, *374*, 20150138.
- (7) Rambaran, R. N.; Serpell, L. C. Amyloid Fibrils: Abnormal Protein Assembly. *Prion* **2008**, *2*, 112–117.
- (8) Maji, S. K.; Perrin, M. H.; Sawaya, M. R.; Jessberger, S.; Vadodaria, K.; Rissman, R. A.; Singru, P. S.; Nilsson, K. P. R.; Simon, R.; Schubert, D. et al. Functional Amyloids as Natural Storage of Peptide Hormones in Pituitary Secretory Granules. *Science* **2009**, *325*, 328–332.
- (9) Dueholm, M. S.; Albertsen, M.; Otzen, D.; Nielsen, P. H. Curli Functional Amyloid Systems Are Phylogenetically Widespread and Display Large Diversity in Operon and Protein Structure. *PLoS One* **2012**, *7*, e51274.
- (10) Ridgley, D. M.; Rippner, C. M. W.; Barone, J. R. Design and Construction of Large Amyloid Fibers. *Fibers* **2015**, *3*, 90–102.

- (11) Knowles, T. P. J.; Mezzenga, R. Amyloid Fibrils as Building Blocks for Natural and Artificial Functional Materials. *Adv. Mater.* **2016**, *28*, 6546–6561.
- (12) Wadsworth, J. D. F.; Joiner, S.; Linehan, J. M.; Desbruslais, M.; Fox, K.; Cooper, S.; Cronier, S.; Asante, E. A.; Mead, S.; Brandner, S. et al. Kuru Prions and Sporadic Creutzfeldt–Jakob Disease Prions Have Equivalent Transmission Properties in Transgenic and Wild-type Mice. *Proc. Natl. Acad. Sci. U. S. A.* **2008**, *105*, 3885–3890.
- (13) Grason, G. M. Perspective: Geometrically Frustrated Assemblies. *J. Chem. Phys.* **2016**, *145*, 110901.
- (14) Hall, D. M.; Bruss, I. R.; Barone, J. R.; Grason, G. M. Morphology Selection via Geometric Frustration in Chiral Filament Bundles. *Nat. Mater.* **2016**, *15*, 727–732.
- (15) Lee, H.-Y.; Oh, H.; Lee, J.-H.; Raghavan, S. R. Shedding Light on Helical Microtubules: Real-time Observations of Microtubule Self-assembly by Light Microscopy. *J. Am. Chem. Soc.* **2012**, *134*, 14375–14381.
- (16) Meldrum, F. C.; Colfen, H. Controlling Mineral Morphologies and Structures in Biological and Synthetic Systems. *Chem. Rev.* **2008**, *108*, 4332–4432.
- (17) Buell, A. K.; Dhulesia, A.; White, D. A.; Knowles, T. P. J.; Dobson, C. M.; Welland, M. E. Detailed Analysis of the Energy Barriers for Amyloid Fibril Growth. *Angew. Chem.-Int. Edit.* **2012**, *51*, 5247–5251.
- (18) Gosal, W. S.; Morten, I. J.; Hewitt, E. W.; Smith, D. A.; Thomson, N. H.; Radford, S. E. Competing Pathways Determine Fibril Morphology in the Self-assembly of β_2 -microglobulin into Amyloid. *J. Mol. Biol.* **2005**, *351*, 850–864.
- (19) Huang, Y.; Wang, D.; Xu, L.; Cong, Y.; Li, J.; Li, L. Multiscale Fibers via Supramolecular Self-assembly of a Fully Rigid, Discotic Aromatic Aramid Molecule. *Eur. Polym. J.* **2013**, *49*, 1682–1687.

- (20) Engelkamp, H.; Middelbeek, S.; Nolte, R. Self-assembly of Disk-shaped Molecules to Coiled-coil Aggregates With Tunable Helicity. *Science* **1999**, *284*, 785–788.
- (21) Jonkheijm, P.; van der Schoot, P.; Schenning, A. P. H.; Meijer, E. W. Probing the Solvent-assisted Nucleation Pathway in Chemical Self-assembly. *Science* **2006**, *313*, 80–83.
- (22) Zhang, J.; Muthukumar, M. Simulations of Nucleation and Elongation of Amyloid Fibrils. *J. Chem. Phys.* **2009**, *130*, 01B610.
- (23) Kashchiev, D.; Auer, S. Nucleation of Amyloid Fibrils. *J. Chem. Phys.* **2010**, *132*, 06B602.
- (24) Šarić, A.; Michaels, T. C. T.; Zacccone, A.; Knowles, T. P. J.; Frenkel, D. Kinetics of Spontaneous Filament Nucleation via Oligomers: Insights from Theory and Simulation. *J. Chem. Phys.* **2016**, *145*, 211926.
- (25) Cabriolu, R.; Kashchiev, D.; Auer, S. Atomistic Theory of Amyloid Fibril Nucleation. *J. Chem. Phys.* **2010**, *133*, 12B602.
- (26) Elemans, J. A. A. W.; Rowan, A. E.; Nolte, R. J. M. Mastering Molecular Matter. Supramolecular Architectures by Hierarchical Self-assembly. *J. Mater. Chem.* **2003**, *13*, 2661–2670.
- (27) Bromley, E. H. C.; Channon, K. J.; King, P. J. S.; Mahmoud, Z. N.; Banwell, E. F.; Butler, M. F.; Crump, M. P.; Dafforn, T. R.; Hicks, M. R.; Hirst, J. D. et al. Assembly Pathway of a Designed α -helical Protein Fiber. *Biophys. J.* **2010**, *98*, 1668–1676.
- (28) Prybytak, P. V.; Frith, W. J.; Cleaver, D. J. Hierarchical Self-assembly of Chiral Fibres from Achiral Particles. *Interface Focus* **2012**, *2*, 651–657.
- (29) Morphew, D.; Chakrabarti, D. Supracolloidal Reconfigurable Polyhedra via Hierarchical Self-assembly. *Soft Matter* **2016**, *12*, 9633–9640.

- (30) Haxton, T. K.; Whitelam, S. Do Hierarchical Structures Assemble Best via Hierarchical Pathways? *Soft Matter* **2013**, *9*, 6851–6861.
- (31) Ogi, S.; Stepanenko, V.; Sugiyasu, K.; Takeuchi, M.; Würthner, F. Mechanism of Self-assembly Process and Seeded Supramolecular Polymerization of Perylene Bisimide Organogelator. *J. Am. Chem. Soc.* **2015**, *137*, 3300–3307.
- (32) Hsiao, L. C.; Schultz, B. A.; Glaser, J.; Engel, M.; Szakasits, M. E.; Glotzer, S. C.; Solomon, M. J. Metastable Orientational Order of Colloidal Discoids. *Nat. Commun.* **2015**, *6*, 8507.
- (33) Collings, P. J.; Goldstein, J. N.; Hamilton, E. J.; Mercado, B. R.; Nieser, K. J.; Regan, M. H. The Nature of the Assembly Process in Chromonic Liquid Crystals. *Liq. Cryst. Rev.* **2015**, *3*, 1–27.
- (34) Huisman, B. A. H.; Bolhuis, P. G.; Fasolino, A. Phase Transition to Bundles of Flexible Supramolecular Polymers. *Phys. Rev. Lett.* **2008**, *100*, 188301.
- (35) Gay, J. G.; Berne, B. J. Modification of the Overlap Potential to Mimic a Linear Site–Site Potential. *J. Chem. Phys.* **1981**, *74*, 3316–3319.
- (36) Cleaver, D. J.; Care, C. M.; Allen, M. P.; Neal, M. P. Extension and Generalization of the Gay–Berne Potential. *Phys. Rev. E* **1996**, *54*, 559.
- (37) Bates, M. A.; Luckhurst, G. R. Computer Simulation Studies of Anisotropic Systems. XXVI. Monte Carlo Investigations of a Gay–Berne Discotic at Constant Pressure. *J. Chem. Phys.* **1996**, *104*, 6696–6709.
- (38) Chakrabarti, D.; Wales, D. J. Tilted and Helical Columnar Phases for an Axially Symmetric Discoidal System. *Phys. Rev. Lett.* **2008**, *100*, 127801.
- (39) Lydon, J. Chromonic Liquid Crystal Phases. *Curr. Opin. Colloid Interface Sci.* **1998**, *3*, 458–466.

- (40) Allen, M. P.; Tildesley, D. J. *Computer Simulation of Liquids*; Oxford U.P, 1987.
- (41) Kamberaj, H.; Low, R. J.; Neal, M. P. Time Reversible and Symplectic Integrators for Molecular Dynamics Simulations of Rigid Molecules. *J. Chem. Phys.* **2005**, *122*, 224114.
- (42) Miller Iii, T.; Eleftheriou, M.; Pattnaik, P.; Ndirango, A.; Newns, D.; Martyna, G. Symplectic Quaternion Scheme for Biophysical Molecular Dynamics. *J. Chem. Phys.* **2002**, *116*, 8649–8659.
- (43) Smith, W. *Elements of Molecular Dynamics*; 2014.
- (44) Eppenga, R.; Frenkel, D. Monte Carlo Study of the Isotropic and Nematic Phases of Infinitely Thin Hard Platelets. *Mol. Phys.* **1984**, *52*, 1303–1334.
- (45) Chakrabarti, D.; Fejer, S. N.; Wales, D. J. Rational Design of Helical Architectures. *Proc. Natl. Acad. Sci. U. S. A.* **2009**, *106*, 20164–20167.
- (46) Eberly, D. Fitting 3D Data with a Helix. Available at: <http://www.geometrictools.com/Documentation> **1999**,
- (47) Shigeno, M.; Kushida, Y.; Yamaguchi, M. Molecular Switching Involving Metastable States: Molecular Thermal Hysteresis and Sensing of Environmental Changes by Chiral Helicene Oligomeric Foldamers. *Chem. Commun.* **2016**, *52*, 4955–4970.
- (48) Mills, E. A.; Regan, M. H.; Stanic, V.; Collings, P. J. Large Assembly Formation via a Two-step Process in a Chromonic Liquid Crystal. *J. Phys. Chem. B* **2012**, *116*, 13506–13515.

Graphical TOC Entry

